Title

Enhancement of an anti-tumor immune response by transient blockade of central T cell tolerance.

Journal

Journal of Experimental Medicine, 211(5)

Authors

Khan, Imran
Mouchess, Maria
Zhu, Meng-Lei
et al.

Publication Date

2014-05-05

DOI

10.1084/jem.20131889

Peer reviewed

Enhancement of an anti-tumor immune response by transient blockade of central T cell tolerance

Imran S. Khan,[1] Maria L. Mouchess,[1] Meng-Lei Zhu,[3,4] Bridget Conley,[3,4] Kayla J. Fasano,[1] Yafei Hou,[2] Lawrence Fong,[2] Maureen A. Su,[3,4] and Mark S. Anderson[1]

[1]Diabetes Center and [2]Division of Hematology/Oncology, Department of Medicine, University of California, San Francisco, San Francisco, CA 94143
[3]Department of Pediatrics and [4]Department of Microbiology/Immunology, School of Medicine, and Lineberger Comprehensive Cancer Center, University of North Carolina, Chapel Hill, NC 27599

Thymic central tolerance is a critical process that prevents autoimmunity but also presents a challenge to the generation of anti-tumor immune responses. Medullary thymic epithelial cells (mTECs) eliminate self-reactive T cells by displaying a diverse repertoire of tissue-specific antigens (TSAs) that are also shared by tumors. Therefore, while protecting against autoimmunity, mTECs simultaneously limit the generation of tumor-specific effector T cells by expressing tumor self-antigens. This ectopic expression of TSAs largely depends on autoimmune regulator (Aire), which is expressed in mature mTECs. Thus, therapies to deplete *Aire*-expressing mTECs represent an attractive strategy to increase the pool of tumor-specific effector T cells. Recent work has implicated the TNF family members RANK and RANK-Ligand (RANKL) in the development of *Aire*-expressing mTECs. We show that in vivo RANKL blockade selectively and transiently depletes *Aire* and TSA expression in the thymus to create a window of defective negative selection. Furthermore, we demonstrate that RANKL blockade can rescue melanoma-specific T cells from thymic deletion and that persistence of these tumor-specific effector T cells promoted increased host survival in response to tumor challenge. These results indicate that modulating central tolerance through RANKL can alter thymic output and potentially provide therapeutic benefit by enhancing anti-tumor immunity.

CORRESPONDENCE
Mark S. Anderson:
manderson@diabetes.ucsf.edu

Abbreviations used: Aire, autoimmune regulator; cTEC, cortical thymic epithelial cell; IRBP, interphotoreceptor retinoid-binding protein; mTEC, medullary thymic epithelial cell; OPG, Osteoprotegerin; TSA, tissue-specific antigen.

Medullary thymic epithelial cells (mTECs) contribute to self-tolerance through the ectopic expression of tissue-specific antigens (TSAs) in the thymus (Derbinski et al., 2001; Anderson et al., 2002; Metzger and Anderson, 2011). This TSA expression in mTECs is largely dependent on autoimmune regulator (Aire), which is expressed in mature mTECs (Gäbler et al., 2007; Gray et al., 2007; Metzger and Anderson, 2011). Through the recognition of TSAs, developing autoreactive T cells are either negatively selected from the pool of developing thymocytes or recruited into the regulatory T (T reg) cell lineage (Liston et al., 2003; Anderson et al., 2005; DeVoss et al., 2006; Shum et al., 2009; Taniguchi et al., 2012; Malchow et al., 2013). The overall importance of this process is underscored by the development of a multi-organ autoimmune syndrome in patients or mice with defective *AIRE* expression (Consortium, 1997; Nagamine et al., 1997; Anderson et al., 2002).

Although central tolerance provides protection against autoimmunity, this process also represents a challenge for anti-tumor immunity (Kyewski and Klein, 2006; Malchow et al., 2013). Because many of the TSAs expressed in the thymus are also expressed in tumors, high-affinity effector T cells capable of recognizing tumor self-antigens may normally be deleted in the thymus (Bos et al., 2005; Cloosen et al., 2007; Träger et al., 2012; Zhu et al., 2013). Transiently suppressing central tolerance by depleting mTECs or modulating *Aire* expression may provide a

I.S. Khan and M.L. Mouchess contributed equally to this paper.

The Rockefeller University Press $30.00
J. Exp. Med. 2014 Vol. 211 No. 5 761–768
www.jem.org/cgi/doi/10.1084/jem.20131889

The Journal of Experimental Medicine

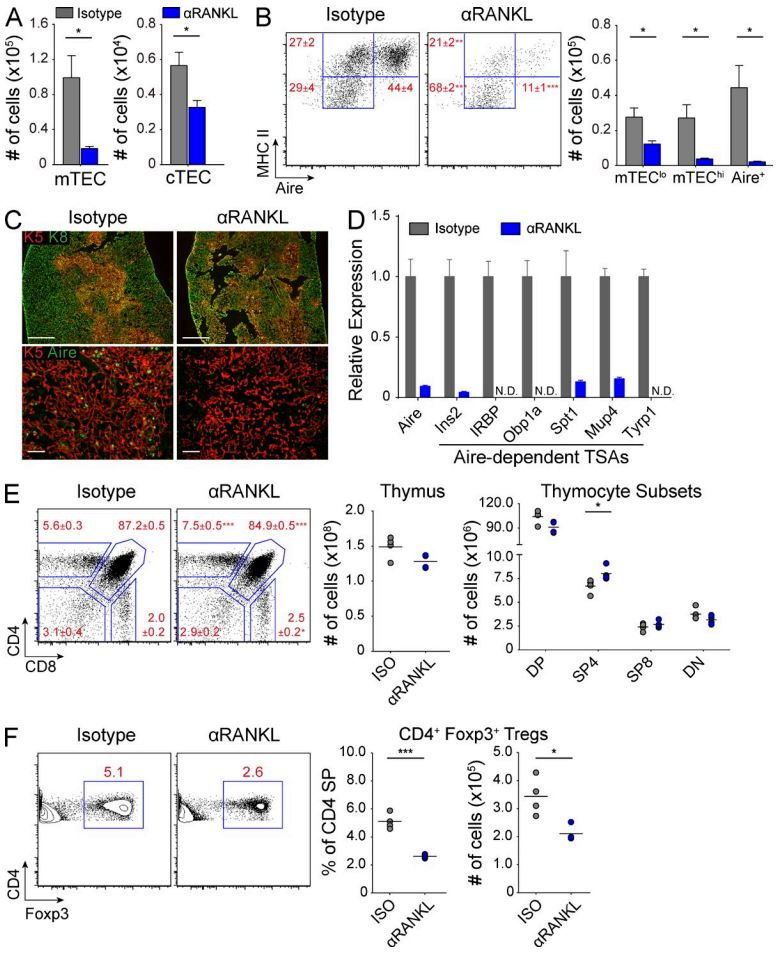

Figure 1. Selective depletion of mTECs with anti-RANKL blockade. (A) Wild-type mice were treated for 2 wk with either isotype (gray) or anti-RANKL (αRANKL, blue) antibody, and absolute numbers of mTECs and cTECs were enumerated by flow cytometry. Bar graphs of total cell numbers are depicted by mean ± SEM. (B) Representative flow cytometry plots of mTECs in A showing relative composition of mTEC subsets. Values represent mean ± SEM. Bar graphs (right) of total cell numbers of each mTEC subset depicted by mean ± SEM. (C) Top panels show immunostaining for keratin-8 (green) and keratin-5 (red) on thymic sections, and bottom panels show immunostaining for keratin-5 (red) and Aire (green). Bars: (top) 500 µm; (bottom) 50 µm. (D) Gene expression analysis on mTECs sorted from wild-type mice treated with either isotype (gray) or anti-RANKL (blue) antibody. Results standardized to Cyclophilin A and normalized to isotype-treated mice with bars depicting mean ± SD. (E) Representative flow cytometry plots of thymocytes from antibody-treated wild-type mice. Values depict mean ± SD. Total thymocyte numbers (right) are indicated with each circle depicting an individual animal and bars showing the mean. (F) Flow cytometric analysis of Foxp3 staining in CD4 SP thymocytes from E. Plots (right) show percentage and number of thymic CD4+ Foxp3+ cells, with bars showing the mean. Data shown in Fig. 1 is representative of two to four independent experiments containing three or more individual mice within each group. *, $P \leq 0.05$; ***, $P \leq 0.001$, Student's *t* test.

therapeutic window for the generation of T cells capable of recognizing tumor self-antigens. Many current cancer immune therapies rely on activating relatively weak tumor-specific T cell responses through modulating peripheral tolerance (Swann and Smyth, 2007; Chen and Mellman, 2013). In contrast, manipulation of central tolerance has the potential to increase the pool and affinity of effector T cells that can recognize and contribute to effective anti-tumor responses. Furthermore, such high-affinity, self-reactive T cells may be more resistant to peripheral tolerance mechanisms that typically restrain an anti-tumor response (Swann and Smyth, 2007). Thus, the development of methods that selectively and transiently deplete *Aire*-expressing mTECs may be an attractive method to enhance tumor-specific immune responses.

Previous work has identified agents that can inhibit the growth and development of TECs such as corticosteroids, cyclosporine, and some inflammatory cytokines (Anz et al., 2009; Fletcher et al., 2009). Despite their clear inhibitory effects on TECs, however, these agents do not appear to have selectivity for blocking mTEC development. Interestingly, recent studies have demonstrated a role for TNF family member pairs RANK–RANKL and CD40-CD40L in the embryological development of Aire$^+$ mTECs (Rossi et al., 2007; Akiyama et al., 2008; Hikosaka et al., 2008; Roberts et al., 2012). Recent work has also demonstrated that mTECs in particular have a relatively fast turnover in adult mice with an estimated half-life of ~2 wk (Gäbler et al., 2007; Gray et al., 2007). Given these findings, we speculated that in vivo blockade of RANKL in adult hosts could both selectively and transiently inhibit the development and turnover of mTECs with potential to alter central T cell tolerance. To this end, we performed in vivo RANKL blockade in adult mice and investigated its effects on both TECs and developing thymocytes. We show that anti-RANKL treatment not only depleted mTECs but could also be used therapeutically to break central tolerance and, as a result, increase the generation of tumor-specific T cells.

RESULTS AND DISCUSSION

Depletion of mTECs with RANKL blockade

The RANK–RANKL signaling pathway is important for mTEC development, but it remains unclear what impact perturbation of this pathway might have on the adult thymus. Previous work has linked the RANK–RANKL pathway to the development of *Aire*-expressing mTECs (Rossi et al., 2007; Akiyama et al., 2008; Hikosaka et al., 2008; Roberts et al., 2012), and we hypothesized that treating mice with blocking anti-RANKL antibody would decrease Aire$^+$ mTECs.

We treated wild-type mice with either anti-RANKL or isotype control antibody for 2 wk and harvested their thymi for analysis. Interestingly, although mice treated with anti-RANKL showed only a modest loss of cortical thymic epithelial cell (cTEC) cellularity, they exhibited a severe depletion of >80% of mTECs (Fig. 1 A). Using MHC II and Aire as markers of mTEC maturation (Gäbler et al., 2007; Gray et al., 2007), we further analyzed the immature mTEC^{lo} (MHC II^{lo} Aire^{-}), intermediate mTEC^{hi} (MHC II^{hi} Aire^{-}), and mature Aire^{+} mTEC subsets (MHC II^{hi} Aire^{+}). The relative mTEC composition in anti-RANKL–treated mice revealed a substantial loss of Aire^{+} and mTEC^{hi} cells along with enrichment of the remaining mTEC^{lo} cells (Fig. 1 B). Although absolute numbers of mTECs were decreased across all mTEC subsets, mTEC depletion was mostly due to the loss of >90% of all Aire^{+} and mTEC^{hi} cells (Fig. 1 B). Immunostaining revealed a slight decrease in the density of keratin-5^{+} (K5) cells in the medulla of anti-RANKL–treated mice, whereas Aire^{+} cells were nearly undetectable (Fig. 1 C). Importantly, staining for keratin-8 (K8) and K5 showed that the overall corticomedullary thymic architecture was preserved despite the loss of mature mTECs (Fig. 1 C). Furthermore, consistent with the loss of the Aire^{+} and mTEC^{hi} subsets, Aire-dependent TSA gene expression in sorted mTECs was decreased in anti-RANKL–treated mice (Fig. 1 D).

Next, we characterized the impact of anti-RANKL–mediated mTEC depletion on thymocyte selection. In the polyclonal T cell repertoire of wild-type mice treated with anti-RANKL, we observed a modest increase in frequencies of both CD4 single-positive (SP) and CD8 SP thymocytes, consistent with a lack of negative selection (Fig. 1 E). Importantly, anti-RANKL–treated mice showed only a slight reduction in the frequency of double-positive thymocytes while absolute numbers were maintained, confirming normal positive selection. In addition, total thymocyte numbers were also maintained in mice treated with anti-RANKL (Fig. 1 E). Furthermore, anti-RANKL–treated mice showed a 50% reduction of Foxp3^{+} T reg cells within the CD4 SP subset (Fig. 1 F).

Given the dramatic impact of RANKL blockade on mTECs, we sought to determine whether this effect could be reversed in the context of increased RANK signaling. Osteoprotegerin (OPG; Tnfrsf11b) is a soluble decoy receptor for RANKL and its role as a negative regulator of RANK signaling has been well described in bone physiology (Kearns et al., 2008). Interestingly, in sorted wild-type mTECs, OPG expression was up-regulated in MHC II^{hi} mTECs when compared with MHC II^{lo} mTECs (Fig. 2 A). To test whether OPG negatively regulates RANK–RANKL signaling in mTECs, we analyzed thymi from *OPG*$^{-/-}$ mice. While cTEC cellularity was increased threefold in *OPG*$^{-/-}$ mice, mTEC cellularity was increased by nearly 10-fold when compared with *OPG*$^{+/+}$ mice (Fig. 2 B). Although absolute numbers of all mTEC subsets were increased in *OPG*$^{-/-}$ mice, we observed an enrichment of Aire^{+} mTECs and a proportional loss of the mTEC^{lo} subset (Fig. 2 C). Immunostaining of K8 and K5 showed that *OPG*$^{-/-}$ thymi maintained their corticomedullary thymic architecture despite these changes in TEC cellularity and mTEC composition (Fig. 2 D).

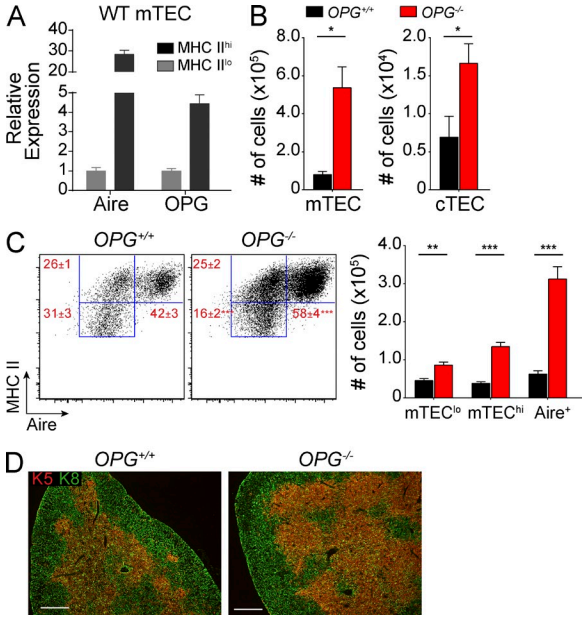

Figure 2. Increased Aire^{+} mTECs in OPG$^{-/-}$ mice. (A) Quantitative PCR analysis of Aire and OPG gene expression in MHC II^{lo} and MHC II^{hi} mTECs sorted from wild-type B6 mice. Results standardized to Cyclophilin A and normalized to MHC II^{lo}, with error bars depicting mean ± SD. (B) Absolute numbers of mTECs and cTECs in OPG$^{+/+}$ (black) and OPG$^{-/-}$ (red) mice were enumerated by flow cytometry. Bar graphs of total cell numbers are depicted by mean ± SEM. (C) Representative flow cytometry plots of mTECs in B showing relative composition of indicated mTEC subsets. Values depict mean ± SEM. Bar graphs (right) depict total cell numbers of each mTEC subset and indicate mean ± SEM. (D) Immunostaining for keratin-8 (green) and keratin-5 (red) on frozen thymic sections from OPG$^{+/+}$ and OPG$^{-/-}$ mice. Data are representative of at least three independent experiments with at least three mice per group. *, P ≤ 0.05; **, P ≤ 0.01; ***, P ≤ 0.001, Student's *t* test. Bars, 500 µm.

Collectively, these data suggest that RANK–RANKL–OPG interactions regulate both TEC cellularity and mTEC maturation, and are particularly important for the induction of Aire^{+} mTECs. Furthermore, anti-RANKL treatment selectively targeted mature mTECs and altered negative selection without affecting the development of new thymocytes.

Regeneration of mTECs after withdrawal of anti-RANKL

We next examined the kinetics of mTEC recovery after withdrawal from anti-RANKL blockade. After a 2-wk treatment window, we harvested mice at 2-wk intervals and observed gradual recovery of the mTEC^{hi} and Aire^{+} subsets (Fig. 3, A and B). By 10 wk, we observed the complete recovery of all mTEC subsets and a normal level of *Aire* expression after anti-RANKL treatment (Fig. 3 B). Interestingly, the pattern of mTEC recovery appeared consistent with published reports of mTEC^{lo} cells giving rise to mTEC^{hi} cells before the induction of Aire^{+} mTECs (Fig. 3 B; Gäbler et al., 2007; Gray et al., 2007; Rossi et al., 2007). Notably, thymi from anti-RANKL– and

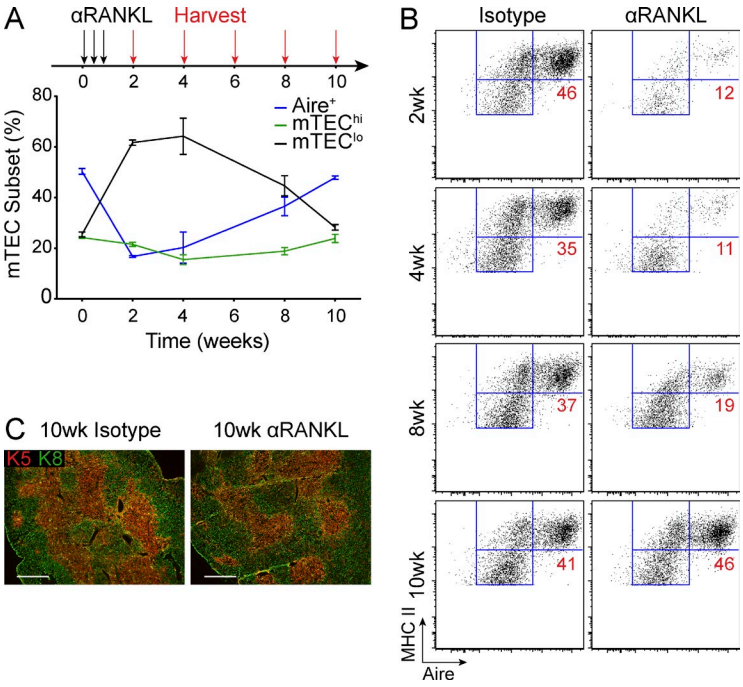

Figure 3. Regeneration of mTECs after anti-RANKL withdrawal. (A) Experimental layout for analysis of mTEC recovery after anti-RANKL withdrawal. Wild-type mice were treated for 1 wk with isotype or anti-RANKL (black arrows) and harvested at indicated time points (red arrows). Graph (bottom) depicts relative composition of mTEC^{lo} mTEC^{hi} and Aire$^+$ mTECs at each time point in anti-RANKL–treated mice. Values represent mean ± SEM. (B) Representative flow cytometry plot of mTECs from each of the indicated time points from A. Values represent the frequency of Aire$^+$ mTECs. (C) Immunostaining for keratin-8 (green) and keratin-5 (red) on thymic sections from isotype or anti-RANKL–treated mice harvested at 10 wk. Bars, 500 µm. Data shown is representative of at least two independent experiments with three to five mice per group.

isotype-treated mice at 10 wk were indistinguishable by immunostaining (Fig. 3 C). Thus, anti-RANKL–mediated mTEC depletion is a transient phenomenon with return of normal thymic composition after withdrawal of antibody treatment.

Manipulation of thymic negative selection with RANKL blockade

To further characterize the impact of anti-RANKL treatment on negative selection, we first used the *OT-II* CD4$^+$ TCR *x RIP-mOVA* double transgenic mouse model. *RIP-mOVA* transgenic mice express a membrane form of OVA under the control of the rat insulin promoter which results in its expression in both the pancreatic islets and in mTECs (Anderson et al., 2005). When the *OT-II* CD4$^+$ TCR transgenic line is crossed to the *RIP-mOVA* transgenic line, OVA-specific *OT-II* T cells are deleted in the thymus (Anderson et al., 2005). We treated both *OT-II* and *OT-II x RIP-mOVA* mice with either anti-RANKL or isotype control antibody and performed thymocyte analysis. Consistent with previous reports, *OT-II x RIP-mOVA* mice treated with control antibody showed a significant

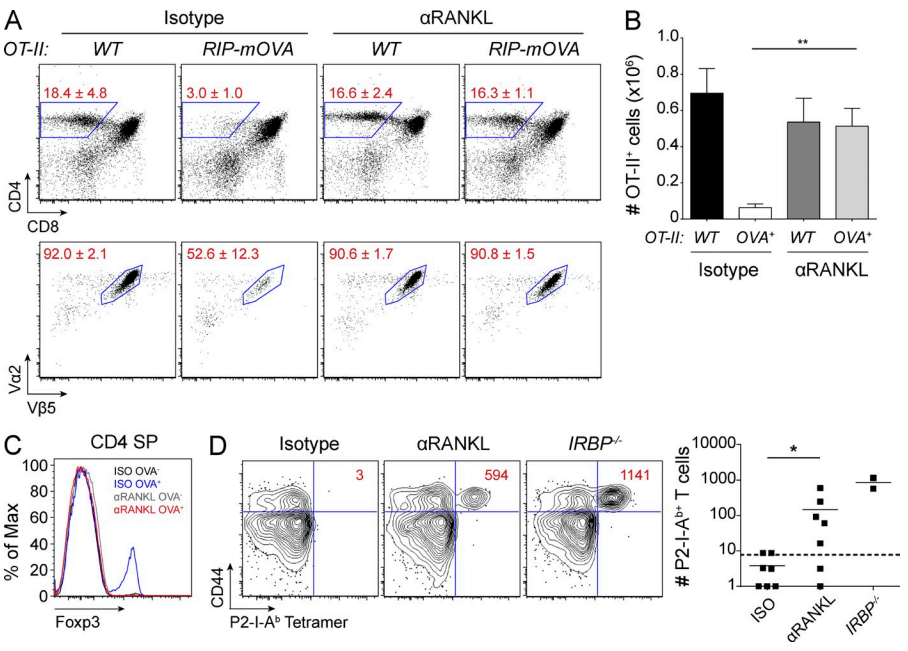

Figure 4. Anti-RANKL–mediated mTEC ablation leads to altered negative selection. (A) *OT-II* and *OT-II x RIP-mOVA* mice were harvested after 2 wk of indicated antibody treatment. Percentages of CD4 SP (top) and OT-II clonotype-specific (bottom) thymocytes are shown. Values represent mean ± SD. (B) Quantification of OT-II clonotype-specific CD4 SP cells from A. Graph shows mean ± SEM. **, $P \leq 0.01$, Student's *t* test. (C) Representative histograms for Foxp3 staining in CD4 SP events from A. (D) Wild-type mice were treated with isotype or anti-RANKL antibody for 3 wk, immunized with P2 peptide, and then harvested 10 d later for tetramer analysis. Representative flow cytometry plots of CD4$^+$ T cells are shown for each condition. Values indicate absolute numbers of CD44$^+$ P2-I-A^b–specific T cells. *IRBP*$^{-/-}$ mice were included as positive controls. Each dot on the graph represents an individual mouse, bars show mean, and the dotted line represents the limit of detection. Data shown is representative of two to three independent experiments. *, $P \leq 0.05$, Mann-Whitney test.

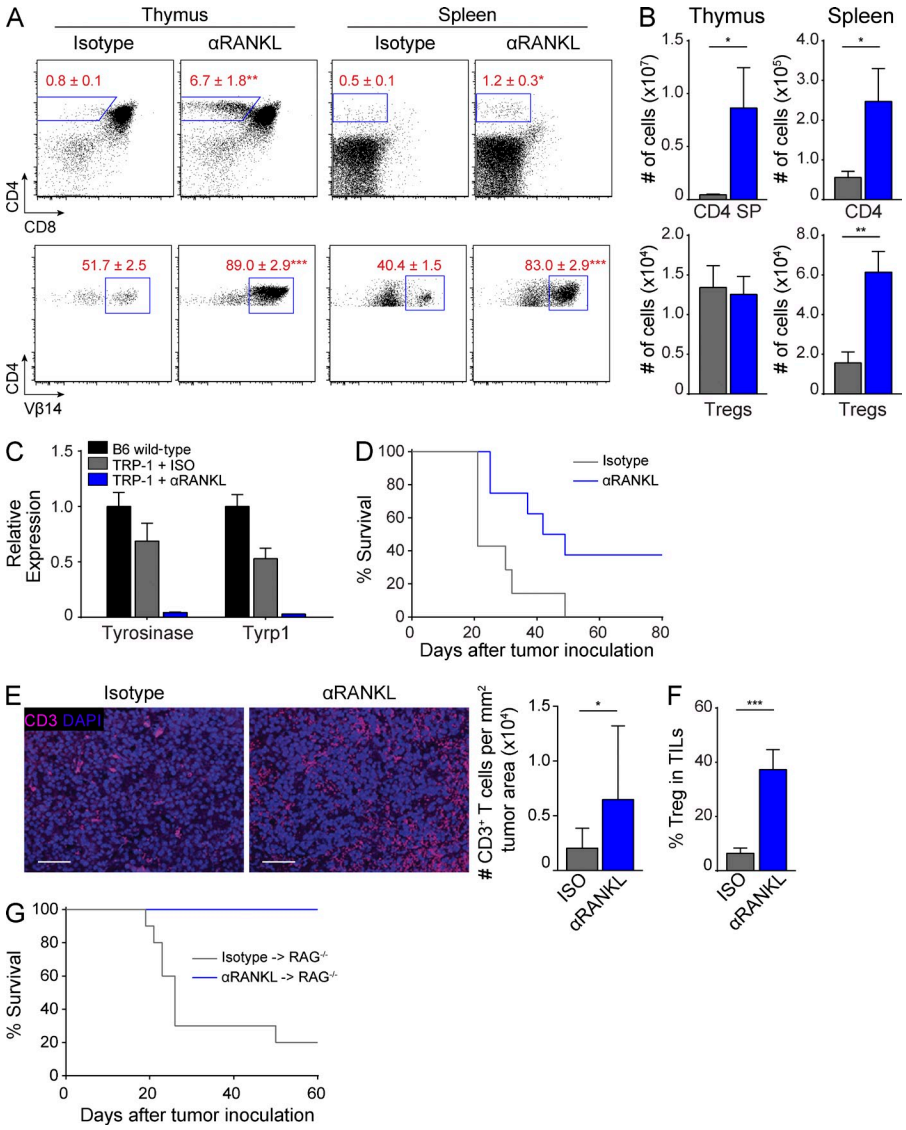

Figure 5. RANKL blockade increases anti-melanoma immune response. (A and B) *RAG1*$^{-/-}$ *x TRP-1* TCR Tg mice were treated with isotype or anti-RANKL antibody for 2 wk and thymus and spleen were harvested for analysis. Flow cytometry plots in A show percentage of CD4$^+$ (top) and CD4-gated Vβ14$^+$ (bottom) T cells. Bar graphs in B show quantification of data in A. Values represent mean ± SEM. *, P ≤ 0.05; **, P ≤ 0.01; ***, P ≤ 0.001, Student's *t* test. Data shown is representative of at least three independent experiments with *n* = 4–7 mice per group. (C) Ear skin from mice treated with isotype (gray) or anti-RANKL (blue) antibody was analyzed by qPCR for Tyrosinase and Tyrp1 expression. Results standardized to β2m and normalized to untreated B6 wild-type mice (black) with bars depicting mean ± SD. (D) Survival curves of *RAG1*$^{-/-}$ *x TRP-1* TCR Tg mice inoculated with B16 melanoma after treatment with isotype (gray) or anti-RANKL (blue) antibody, *n* = 7–8 mice for each group. P ≤ 0.05, Log-rank test. Data shown is representative of four independent experiments. (E) Tumor sections from isotype or anti-RANKL–treated mice in D were immunostained for CD3 (pink) with DAPI counterstain (purple). Bars, 50 µm. Mean densities of CD3$^+$ cells per tumor area are quantified on the right. Four sections were evaluated for each treatment group and 6 imaging fields were randomly scored from each section. Graphs depict mean ± SEM. *, P ≤ 0.05, Student's *t* test. (F) *RAG1*$^{-/-}$ *x TRP-1* TCR Tg mice were inoculated with B16 melanoma after treatment with isotype (gray) or anti-RANKL (blue) antibody. Mice were harvested at 21 d after tumor inoculation and tumor-infiltrating lymphocytes (TILs) were analyzed by flow cytometry. Graph depicts percentage of Foxp3$^+$ CD25$^+$ T reg cells among CD4$^+$ T cells. Values represent mean ± SEM. ***, P ≤ 0.001, Student's *t* test. Data shown is *n* = 7–9 mice per group pooled from two independent experiments. (G) Survival curves of *RAG1*$^{-/-}$ recipients inoculated with B16 melanoma after adoptive transfer of splenocytes from either anti-RANKL (blue)– or isotype (gray)–treated *RAG1*$^{-/-}$ *x TRP-1* TCR Tg mice, *n* = 10 mice for each group. P ≤ 0.001, Log-rank test. Data shown is representative of two independent experiments.

reduction in the proportions of CD4 SP thymocytes and also had decreased frequencies and numbers of *OT-II*$^+$ T cells (Fig. 4, A and B; Anderson et al., 2005). In contrast, thymocyte profiles of anti-RANKL–treated *OT-II x RIP-mOVA* mice were indistinguishable from that of *OT-II* mice, demonstrating that RANKL blockade prevented thymic deletion of *OT-II* T cells yet allowed their positive selection (Fig. 4, A and B). We also observed a loss of thymic T reg cell development in these mice, which suggested a loss of cognate antigen (OVA) expression from mTECs within the thymus (Fig. 4 C).

To expand these observations to the polyclonal T cell repertoire, we analyzed the development of Aire-dependent autoreactive T cells using a tetramer enrichment protocol. Previously, we had shown that T cells specific for the self-antigen interphotoreceptor retinoid-binding protein (IRBP) are deleted in thymus of *Aire*$^{+/+}$ mice, whereas these cells escape deletion in *Aire*$^{-/-}$ mice and cause autoimmune uveitis (DeVoss et al., 2006; Taniguchi et al., 2012). Through the use of an IRBP peptide class II tetramer, P2-I-A^b, such autoreactive CD4$^+$ T cells can be detected in *Aire*$^{-/-}$ mice. Given both the severe depletion of Aire$^+$ mTECs and the loss of thymic *IRBP* expression in anti-RANKL–treated mice, we hypothesized that P2-I-A^b–specific T cells could be detected in treated mice. After treating wild-type mice with anti-RANKL antibody, we immunized mice with a MHC II–binding IRBP peptide epitope (P2) to expand T cells for detection. 10 d after immunization, lymph nodes and spleen were pooled for the enumeration of CD4$^+$ P2-I-A^b–specific T cells by flow cytometry. Consistent with the loss of Aire$^+$ mTECs, tetramer analysis of anti-RANKL–treated mice revealed an expansion of CD4$^+$ P2-I-A^b–specific T cells

(Fig. 4 D). Overall, these data show a clear defect in negative selection associated with the loss of Aire$^+$ mTECs in anti-RANKL–treated mice.

Treatment with anti-RANKL enhances anti-tumor immunity

Given its ability to selectively block mTECs and central tolerance, we next sought to determine whether anti-RANKL treatment could be used to therapeutically enhance anti-tumor immunity. Previous work has shown that many tumor self-antigens are expressed by mTECs as TSAs, and that high-affinity T cells capable of recognizing these tumor self-antigens are efficiently deleted in the thymus (Bos et al., 2005; Träger et al., 2012; Zhu et al., 2013). To test whether anti-RANKL treatment could rescue tumor self-antigen–specific T cells from thymic deletion, we used the *TRP-1* CD4$^+$ TCR transgenic mouse model which generates T cells specific for the melanoma antigen TRP-1 (Tyrp1; Muranski et al., 2008). TRP-1 is expressed in B16 melanoma cells, and *TRP-1* T cells are efficacious against established B16 melanoma tumors (Muranski et al., 2008). Importantly, mTECs endogenously express *TRP-1* in an Aire-dependent manner, such that TRP-1–specific T cells are deleted in the thymi of *Aire*-sufficient, *TRP-1*–sufficient hosts (Muranski et al., 2008; Zhu et al., 2013). Given the depletion of Aire$^+$ mTECs and loss of thymic *TRP-1* expression in anti-RANKL–treated mice (Fig. 1 D), we hypothesized that anti-RANKL treatment could rescue *TRP-1* T cells from thymic deletion. We treated *RAG1*$^{-/-}$ *x TRP-1* TCR transgenic mice with either anti-RANKL or control antibody and harvested their thymi and spleens for analysis. Consistent with previous reports, isotype-treated mice showed efficient deletion of CD4 SP T cells in the thymus (Fig. 5 A; Muranski et al., 2008; Zhu et al., 2013). In contrast, anti-RANKL treatment prevented deletion of CD4 SP cells and also resulted in a much higher percentage of Vβ14$^+$ T cells (Fig. 5, A and B). Furthermore, *TRP-1* T cells were detectable in the spleens of anti-RANKL–treated mice and also expressed higher levels of the Vβ14 TCR (Fig. 5, A and B). In addition, qPCR analysis revealed a loss of *Tyrosinase* and *Tyrp1* expression in the ear skin of anti-RANKL–treated mice which appeared consistent with the destruction of melanocytes by *TRP-1* T cells (Fig. 5 C).

Next, we challenged anti-RANKL–treated *RAG1*$^{-/-}$ *x TRP-1* mice with B16 melanoma to determine whether a limited break in central tolerance could improve overall survival. We observed a statistically significant increase in the survival of anti-RANKL–treated mice compared with the isotype-treated cohort (Fig. 5 D). We also found evidence of an enhanced T cell response in anti-RANKL–treated mice by measuring CD3$^+$ T cell infiltrates within the tumors of these mice (Fig. 5 E). Of note, given the overall increase in T reg cells in the spleen and tumors of anti-RANKL–treated mice, it appears unlikely that the survival benefit observed in *TRP-1* mice is due to differences in T reg cell numbers (Fig. 5, B and F). Furthermore, to exclude potential effects of anti-RANKL antibody on the tumor microenvironment, we performed adoptive transfer studies in which splenocytes from antibody-treated *RAG1*$^{-/-}$ *x TRP-1* mice were transferred into *RAG1*$^{-/-}$ mice. When challenged with B16 melanoma, recipients of splenocytes from anti-RANKL–treated donors again showed a statistically significant increase in survival (Fig. 5 G). Collectively, these data demonstrate that short-term, reversible RANKL blockade of mTEC development can be used to create a therapeutic window that allows tumor self-antigen–specific T cells to escape thymic deletion. Furthermore, the generation of these high-affinity tumor-specific T cells confers a survival benefit in a melanoma tumor model.

In conclusion, our findings provide strong evidence that mTECs can be selectively and therapeutically targeted by RANKL blockade in adult mice and that anti-RANKL can be used as an approach to enhance anti-tumor responses. To date, previous efforts on the therapeutic manipulation of TECs have shown global effects that involve both cTECs and mTECs and disrupt thymocyte development (Fletcher et al., 2009). The selectivity for mTECs with anti-RANKL thus provides evidence that central tolerance can be transiently suppressed in adult hosts while maintaining T cell generation. Although autoimmunity is a dangerous potential consequence of this approach, the treatment may also be an attractive new method to help break tolerance for cancer immunotherapy. Interestingly, although we could detect an expansion of retina-specific T cells in anti-RANKL–treated mice, we did not observe development of spontaneous uveitis (unpublished data), suggesting that this brief window of central tolerance suppression was countered by peripheral tolerance mechanisms such as T reg cells which existed before treatment. Importantly, we find that the medullary epithelial compartment of the thymus recovers after withdrawal of anti-RANKL antibody and, thus, only a transient window of central tolerance suppression occurs. This window may be an attractive feature of this approach, especially if coupled with methods that preferentially expand tumor-specific T cells over pathogenic autoreactive T cells. Currently, there has been intense interest and progress in manipulating peripheral tolerance for immunotherapy (Chen and Mellman, 2013). Given our results, it will also be of interest to determine if a combination of methods that target both central and peripheral tolerance could further enhance anti-tumor immune responses. Finally, it is important to note that our results also have implications for patients in the clinical setting receiving denosumab, a humanized monoclonal antibody that blocks RANKL which is widely used in the treatment of osteoporosis in adults (Cummings et al., 2009). Further study will be needed in such patients regarding their susceptibility to autoimmunity and for other potential defects in central tolerance.

MATERIALS AND METHODS

Mice. C57BL/6, *B6.RAG1*$^{-/-}$ *Tyrp1*$^{B\text{-}w}$ *TRP-1 TCR* transgenic, and *B6.OPG*$^{-/-}$ mice were purchased from The Jackson Laboratory. Mice were treated intraperitoneally with 100 µg anti-RANKL (IK22/5) or isotype control (2A3; Bio X Cell) antibody three times per week as stated in the text. *B6.OT-II*, *B6.RIP-mOVA*, and *B6.IRBP*$^{-/-}$ mice were described previously (Anderson et al., 2005; DeVoss et al., 2006). Mice were treated at 3–5 wk of age and harvested at time points indicated in the text. All mice were housed and bred in specific pathogen-free conditions in animal facilities at UCSF or

UNC, Chapel Hill. Animal experiments were approved by the Institutional Animal Care and Use Committee (IACUC) at UCSF or UNC, Chapel Hill.

Quantitative PCR. RNA was extracted from sorted mTECs using the RNeasy Micro Plus kit (QIAGEN) and cDNA was synthesized with the Invitrogen Superscript III kit. TaqMan gene expression assays (Applied Biosystems) were used for all targets.

Histology and immunofluorescence. Thymi were harvested and embedded in O.C.T. media (Tissue-Tek). 8-µm frozen thymic sections were fixed in 100% acetone, blocked, and stained for keratin-5, keratin-8 (Abcam), or Aire (eBioscience). Secondary antibodies were purchased from Invitrogen. Thymic sections were visualized using a widefield microscope (Apotome; Carl Zeiss). For tumor immunostaining, tumors were harvested and fixed in 10% formalin as previously described (Zhu et al., 2013). Fixed tumors were embedded in paraffin and sectioned for staining with anti-CD3 antibody and counterstained with DAPI. Tumor sections were visualized using a fluorescent microscope (BX60; Olympus) and analyzed using ImageJ software (National Institutes of Health).

Flow cytometry. TECs were isolated as previously described (Gardner et al., 2008). In brief, thymi were minced and digested with DNase I and Liberase TM (Roche) before gradient centrifugation with Percoll PLUS (GE Healthcare). Enriched stromal cells were stained with the indicated surface marker antibodies (BioLegend). mTECs were defined as $CD45^-$, $EpCAM^+$, MHC II^+, $Ly51^-$ events and cTECs were defined as $CD45^-$, $EpCAM^+$, MHC II^+, $Ly51^+$ events. For lymphocyte staining, all surface marker antibodies were obtained from BioLegend. For intracellular staining, cells were stained using the Foxp3 Staining Buffer Set and stained with anti-Foxp3 or anti-Aire (eBioscience). All data were collected using a flow cytometer (LSR II; BD) and analyzed with either FlowJo software (Tree Star) or FACS Diva (BD). Cell sorting was performed using a FACS Aria III cell sorter (BD).

IRBP P2 peptide immunization and tetramer analysis. Mice were immunized with 100 µg P2 peptide (IRBP; aa 271–290) emulsified in complete Freund's adjuvant as described previously (Taniguchi et al., 2012). Tetramer analysis was performed on pooled lymph nodes and spleen from treated mice 10 d after immunization. P2-I-A^b tetramer was generated by the National Institutes of Health Tetramer Core Facility, and tetramer staining was performed as described previously (Taniguchi et al., 2012). After tetramer enrichment, cells were stained with antibodies for flow cytometry, and counting beads (Invitrogen) were used to enumerate $tetramer^+$ cells.

B16 melanoma tumor challenge. *B6.RAG1*$^{-/-}$*TRP-1 TCR* transgenic mice were injected subcutaneously in the left flank with 1.0×10^5 B16 melanoma cells. For adoptive transfer studies, spleens from donor mice were pooled and CD25-depleted before transfer into *B6.RAG1*$^{-/-}$ hosts. Recipient mice were inoculated with 7.5×10^4 B16 melanoma cells 7 d after transfer. Tumor growth was monitored by taking measurements of length (*L*) and width (*W*), and tumor volume was calculated as $LW^2/2$. For generation of survival curves, death was defined as tumor size >1,000 mm^3.

Statistical analysis. Statistical analysis was performed using Prism 6.0 (GraphPad Software). Mann-Whitney Rank sum testing was performed on tetramer analysis. Student's *t* test was performed for TEC and lymphocyte analyses. Log-rank test was performed for Kaplan-Meier survival curves.

We thank T. Metzger, T. LaFlam, M. Cheng, and W. Purtha for critical reading of the manuscript. We thank the National Institutes of Health Tetramer Core Facility for providing tetramer reagent.

This work was supported by the US National Institutes of Health Grants AI097457 (M.S. Anderson) and K12-GM081266 (M.L. Mouchess), and the UCSF Medical Scientist Training Program (I.S. Khan). Flow cytometry data were generated in the UCSF Parnassus Flow Cytometry Core, which is supported by the Diabetes and Endocrinology Research Center (DERC) grant NIH P30 DK063720.

The authors declare no competing financial interests.

Submitted: 6 September 2013
Accepted: 3 April 2014

REFERENCES

Akiyama, T., Y. Shimo, H. Yanai, J. Qin, D. Ohshima, Y. Maruyama, Y. Asaumi, J. Kitazawa, H. Takayanagi, J.M. Penninger, et al. 2008. The tumor necrosis factor family receptors RANK and CD40 cooperatively establish the thymic medullary microenvironment and self-tolerance. *Immunity*. 29:423–437. http://dx.doi.org/10.1016/j.immuni.2008.06.015

Anderson, M.S., E.S. Venanzi, L. Klein, Z. Chen, S.P. Berzins, S.J. Turley, H. von Boehmer, R. Bronson, A. Dierich, C. Benoist, and D. Mathis. 2002. Projection of an immunological self shadow within the thymus by the aire protein. *Science*. 298:1395–1401. http://dx.doi.org/10.1126/science.1075958

Anderson, M.S., E.S. Venanzi, Z. Chen, S.P. Berzins, C. Benoist, and D. Mathis. 2005. The cellular mechanism of Aire control of T cell tolerance. *Immunity*. 23:227–239. http://dx.doi.org/10.1016/j.immuni.2005.07.005

Anz, D., R. Thaler, N. Stephan, Z. Waibler, M.J. Trauscheid, C. Scholz, U. Kalinke, W. Barchet, S. Endres, and C. Bourquin. 2009. Activation of melanoma differentiation-associated gene 5 causes rapid involution of the thymus. *J. Immunol.* 182:6044–6050. http://dx.doi.org/10.4049/jimmunol.0803809

Bos, R., S. van Duikeren, T. van Hall, P. Kaaijk, R. Taubert, B. Kyewski, L. Klein, C.J. Melief, and R. Offringa. 2005. Expression of a natural tumor antigen by thymic epithelial cells impairs the tumor-protective CD4+ T-cell repertoire. *Cancer Res.* 65:6443–6449. http://dx.doi.org/10.1158/0008-5472.CAN-05-0666

Chen, D.S., and I. Mellman. 2013. Oncology meets immunology: the cancer-immunity cycle. *Immunity*. 39:1–10. http://dx.doi.org/10.1016/j.immuni.2013.07.012

Cloosen, S., J. Arnold, M. Thio, G.M. Bos, B. Kyewski, and W.T. Germeraad. 2007. Expression of tumor-associated differentiation antigens, MUC1 glycoforms and CEA, in human thymic epithelial cells: implications for self-tolerance and tumor therapy. *Cancer Res.* 67:3919–3926. http://dx.doi.org/10.1158/0008-5472.CAN-06-2112

Consortium, F.G.A.; Finnish-German APECED Consortium. 1997. An autoimmune disease, APECED, caused by mutations in a novel gene featuring two PHD-type zinc-finger domains. *Nat. Genet.* 17:399–403. http://dx.doi.org/10.1038/ng1297-399

Cummings, S.R., J. San Martin, M.R. McClung, E.S. Siris, R. Eastell, I.R. Reid, P. Delmas, H.B. Zoog, M. Austin, A. Wang, et al. FREEDOM Trial. 2009. Denosumab for prevention of fractures in postmenopausal women with osteoporosis. *N. Engl. J. Med.* 361:756–765. http://dx.doi.org/10.1056/NEJMoa0809493

Derbinski, J., A. Schulte, B. Kyewski, and L. Klein. 2001. Promiscuous gene expression in medullary thymic epithelial cells mirrors the peripheral self. *Nat. Immunol.* 2:1032–1039. http://dx.doi.org/10.1038/ni723

DeVoss, J., Y. Hou, K. Johannes, W. Lu, G.I. Liou, J. Rinn, H. Chang, R.R. Caspi, L. Fong, and M.S. Anderson. 2006. Spontaneous autoimmunity prevented by thymic expression of a single self-antigen. *J. Exp. Med.* 203:2727–2735. http://dx.doi.org/10.1084/jem.20061864

Fletcher, A.L., T.E. Lowen, S. Sakkal, J.J. Reiseger, M.V. Hammett, N. Seach, H.S. Scott, R.L. Boyd, and A.P. Chidgey. 2009. Ablation and regeneration of tolerance-inducing medullary thymic epithelial cells after cyclosporine, cyclophosphamide, and dexamethasone treatment. *J. Immunol.* 183:823–831. http://dx.doi.org/10.4049/jimmunol.0900225

Gäbler, J., J. Arnold, and B. Kyewski. 2007. Promiscuous gene expression and the developmental dynamics of medullary thymic epithelial cells. *Eur. J. Immunol.* 37:3363–3372. http://dx.doi.org/10.1002/eji.200737131

Gardner, J.M., J.J. Devoss, R.S. Friedman, D.J. Wong, Y.X. Tan, X. Zhou, K.P. Johannes, M.A. Su, H.Y. Chang, M.F. Krummel, and M.S. Anderson. 2008. Deletional tolerance mediated by extrathymic Aire-expressing cells. *Science*. 321:843–847. http://dx.doi.org/10.1126/science.1159407

Gray, D., J. Abramson, C. Benoist, and D. Mathis. 2007. Proliferative arrest and rapid turnover of thymic epithelial cells expressing Aire. *J. Exp. Med.* 204:2521–2528. http://dx.doi.org/10.1084/jem.20070795

Hikosaka, Y., T. Nitta, I. Ohigashi, K. Yano, N. Ishimaru, Y. Hayashi, M. Matsumoto, K. Matsuo, J.M. Penninger, H. Takayanagi, et al. 2008. The cytokine RANKL produced by positively selected thymocytes fosters medullary thymic epithelial cells that express autoimmune regulator. *Immunity*. 29:438–450. http://dx.doi.org/10.1016/j.immuni.2008.06.018

Kearns, A.E., S. Khosla, and P.J. Kostenuik. 2008. Receptor activator of nuclear factor kappaB ligand and osteoprotegerin regulation of bone remodeling in health and disease. *Endocr. Rev.* 29:155–192. http://dx.doi.org/10.1210/er.2007-0014

Kyewski, B., and L. Klein. 2006. A central role for central tolerance. *Annu. Rev. Immunol.* 24:571–606. http://dx.doi.org/10.1146/annurev.immunol.23.021704.115601

Liston, A., S. Lesage, J. Wilson, L. Peltonen, and C.C. Goodnow. 2003. Aire regulates negative selection of organ-specific T cells. *Nat. Immunol.* 4:350–354. http://dx.doi.org/10.1038/ni906

Malchow, S., D.S. Leventhal, S. Nishi, B.I. Fischer, L. Shen, G.P. Paner, A.S. Amit, C. Kang, J.E. Geddes, J.P. Allison, et al. 2013. Aire-dependent thymic development of tumor-associated regulatory T cells. *Science.* 339:1219–1224. http://dx.doi.org/10.1126/science.1233913

Metzger, T.C., and M.S. Anderson. 2011. Control of central and peripheral tolerance by Aire. *Immunol. Rev.* 241:89–103. http://dx.doi.org/10.1111/j.1600-065X.2011.01008.x

Muranski, P., A. Boni, P.A. Antony, L. Cassard, K.R. Irvine, A. Kaiser, C.M. Paulos, D.C. Palmer, C.E. Touloukian, K. Ptak, et al. 2008. Tumor-specific Th17-polarized cells eradicate large established melanoma. *Blood.* 112:362–373. http://dx.doi.org/10.1182/blood-2007-11-120998

Nagamine, K., P. Peterson, H.S. Scott, J. Kudoh, S. Minoshima, M. Heino, K.J. Krohn, M.D. Lalioti, P.E. Mullis, S.E. Antonarakis, et al. 1997. Positional cloning of the APECED gene. *Nat. Genet.* 17:393–398. http://dx.doi.org/10.1038/ng1297-393

Roberts, N.A., A.J. White, W.E. Jenkinson, G. Turchinovich, K. Nakamura, D.R. Withers, F.M. McConnell, G.E. Desanti, C. Benezech, S.M. Parnell, et al. 2012. Rank signaling links the development of invariant γδ T cell progenitors and Aire(+) medullary epithelium. *Immunity.* 36:427–437. http://dx.doi.org/10.1016/j.immuni.2012.01.016

Rossi, S.W., M.Y. Kim, A. Leibbrandt, S.M. Parnell, W.E. Jenkinson, S.H. Glanville, F.M. McConnell, H.S. Scott, J.M. Penninger, E.J. Jenkinson, et al. 2007. RANK signals from $CD4^{+}3^{-}$ inducer cells regulate development of Aire-expressing epithelial cells in the thymic medulla. *J. Exp. Med.* 204:1267–1272. http://dx.doi.org/10.1084/jem.20062497

Shum, A.K., J. DeVoss, C.L. Tan, Y. Hou, K. Johannes, C.S. O'Gorman, K.D. Jones, E.B. Sochett, L. Fong, and M.S. Anderson. 2009. Identification of an autoantigen demonstrates a link between interstitial lung disease and a defect in central tolerance. *Sci. Transl. Med.* 1:9ra20. http://dx.doi.org/10.1126/scitranslmed.3000284

Swann, J.B., and M.J. Smyth. 2007. Immune surveillance of tumors. *J. Clin. Invest.* 117:1137–1146. http://dx.doi.org/10.1172/JCI31405

Taniguchi, R.T., J.J. DeVoss, J.J. Moon, J. Sidney, A. Sette, M.K. Jenkins, and M.S. Anderson. 2012. Detection of an autoreactive T-cell population within the polyclonal repertoire that undergoes distinct autoimmune regulator (Aire)-mediated selection. *Proc. Natl. Acad. Sci. USA.* 109:7847–7852. http://dx.doi.org/10.1073/pnas.1120607109

Träger, U., S. Sierro, G. Djordjevic, B. Bouzo, S. Khandwala, A. Meloni, M. Mortensen, and A.K. Simon. 2012. The immune response to melanoma is limited by thymic selection of self-antigens. *PLoS ONE.* 7:e35005. http://dx.doi.org/10.1371/journal.pone.0035005

Zhu, M.L., A. Nagavalli, and M.A. Su. 2013. Aire deficiency promotes TRP-1-specific immune rejection of melanoma. *Cancer Res.* 73:2104–2116. http://dx.doi.org/10.1158/0008-5472.CAN-12-3781